BIOCHEMISTRY
including biophysical chemistry & molecular biology
Article

Biochemistry **2010,** *49,* 3445–3455 3445
DOI: 10.1021/bi902180m

Molecular and Cellular Mechanisms Underlying Neural Tube Defects in the Loop-tail Mutant Mouse†

Michel Gravel,‡ Alexandra Iliescu,‡ Cynthia Horth,‡ Sergio Apuzzo,‡ and Philippe Gros*,‡

‡*Department of Biochemistry and Complex Traits Program, McGill University, Montreal, Quebec, Canada H3G 0B1*

Received December 18, 2009; Revised Manuscript Received February 24, 2010

ABSTRACT: Loop-tail (*Lp*) mice show a very severe neural tube defect (craniorachischisis) caused by mutations in the *Vangl2* gene (D255E, S464N). Mammalian Vangl1 and Vangl2 are membrane proteins that play critical roles in development such as establishment of planar cell polarity (PCP) in epithelial layers and convergent extension movements during neurogenesis and cardiogenesis. Vangl proteins are thought to assemble with other PCP proteins (Dvl, Pk) to form membrane-bound PCP signaling complexes that provide polarity information to the cell. In the present study, we show that Vangl1 is expressed exclusively at the plasma membrane of transfected MDCK cells, where it is targeted to the basolateral membrane. Experiments with an inserted exofacial HA epitope indicate that the segment delimited by the predicted transmembrane domains 1 and 2 is exposed to the extracellular milieu. Comparative studies of the *Lp*-associated pathogenic mutation D255E indicate that the targeting of the mutant variant at the plasma membrane is greatly reduced; the mutant variant is predominantly retained intracellularly in endoplasmic reticulum (ER) vesicles colocalizing with the ER marker calreticulin. In addition, the D255E variant shows drastically reduced stability with a half-life of ~2 h, compared to >9 h for its wild type counterpart and is rapidly degraded in a proteasome-dependent and MG132 sensitive pathway. These findings highlight a critical role for D255 for normal folding and processing of Vangl proteins, with highly conservative substitutions not tolerated at that site. Our study provide an experimental framework for the analysis of human *VANGL* mutations recently identified in familial and sporadic cases of spina bifida.

Neural tube defects (NTDs)[1] are a heterogeneous group of pathologies that occur when the neural tube fails to close properly. NTDs constitute one of the most common congenital abnormalities in humans, occurring in 1 per 1000 live births (*1*). Multiple factors, both genetic and environmental, have been implicated in the etiology of NTDs, underlying the causal heterogeneity of the disorder (*1*, *2*). The study of mouse mutants affected with NTDs has enabled the identification of molecular pathways involved in the complex process of neurulation (*3*). *Loop-tail* (*Lp*) is a semidominant mutation where *Lp*/+ heterozygotes display urogenital defects and a characteristic "looped" tail (*4*), while *Lp*/*Lp* homozygotes display craniorachischisis and die in utero shortly before or at birth. Craniorachischisis is characterized by a completely open neural tube, from the hindbrain region to the most caudal extremity of the embryo, while the forebrain and the midbrain regions are closed properly (*5*−*7*). We have identified *Vangl2* as the gene mutated in the *loop-tail* (*Lp*) mouse model of NTD (*5*, *6*). *Vangl2* RNA is expressed embryonically in several tissues, including robust levels in the neural tube immediately prior to, during and after closure (*5*−*8*). *Vangl2* encodes a membrane protein comprising four putative transmembrane domains and a large intracellular domain with a PDZ-domain-binding motif (PBM) at its carboxy terminus (*9*). Recently, we have shown that the Vangl2 protein is expressed at the plasma membrane of neuroepithelial cells of E10.5 of mouse embryos and is also present at the basolateral membrane of several types of epithelial cells (*8*).

Vangl genes are highly conserved in evolution with members in flies (Vang/Stbm), fish (trilobite/Vangl2), and frogs (Xstbm) (*10*−*13*). In *Drosophila* the Vang/Stbm relative is required for establishing planar cell polarity (PCP) in the developing eye, wing, and leg (*14*, *15*). This process is regulated by membrane-associated signaling complexes composed of Vang/Stbm, the plasma membrane receptor Frizzled (Fz), the cytoplasmic proteins Dishevelled (Dsh/Dvl) and Prickle (Pk), and the atypical cadherins Flamingo/Starry night (Fmi/Stan) and Diego (Dgo) (*16*−*22*). Establishment of PCP involves the redistribution of these proteins; cytoplasmic Dvl and Pk are recruited to the membrane to form asymmetrically distributed membrane complexes with Fz and Stbm/Vang, respectively (*23*). Vangl proteins have been shown to bind both Dvl and Pk (*24*−*27*). In the absence of Vang, Dsh and Pk are mislocalized and PCP signaling is impaired (*25*). Fz and Vang also participate in intercellular PCP signal relay (*28*). In addition, vertebrate relatives of fly PCP genes have been shown to participate in convergent extension (CE) movements during embryogenesis (*29*). CE is the process in which layers of cells intercalate (converge) and become longer (extension) contributing to a variety of morphogenetic processes. CE movements are responsible for the narrowing and

†This work was supported by a research grant to P.G. from the Canadian Institutes of Health Research (MOP-13425). P.G. is a James McGill Professor of Biochemistry.

*To whom all correspondence should be addressed: Philippe Gros, Ph.D., Professor, Department of Biochemistry, McGill University, 3649 Promenade Sir William Osler, Room 366, Montreal, Quebec, Canada, H3G 0B1. Tel.: 514-398-7291. Fax: 514-598-2603. E-mail: philippe.gros@mcgill.ca.

[1]Abbreviations: NTD, neural tube defect; TM, transmembrane; PCP, planar cell polarity; CE, convergent extension.

Published on Web 03/24/2010

lengthening of the neural plate during neural tube closure (*11*, *30*−*32*). Interestingly, mutations in mammalian counterparts of the Drosophila PCP genes *Vangl*, *Fz*, *Dvl*, and *Celsr1* cause severe NTDs (*5*, *6*, *33*−*35*).

In vertebrates, a second *Vangl* gene, *VANGL1*, has been described (*9*, *36*). Vangl1 and Vangl2 proteins are highly similar, including identical major predicted secondary structure features. In mice, *Vangl1* is also expressed in the developing neural tube (ventral neural tube, notochord). *VANGL1* genetically interacts with *VANGL2* and mouse embryos doubly heterozygotes for *Vangl1*/*2* mutations (*Vangl1*$^{+/-}$: *Vangl2*$^{+/-}$) display craniorachischisis (*37*). Moreover, several mutations in sporadic (M328T) and familial (V239I, R274Q) cases of NTDs were identified in the human *VANGL1* gene, including a de novo mutation (V239I) appearing in a familial setting (*38*, *39*). The structural similarity shared by Vangl proteins (*9*), their genetic interaction during neural tube development (*37*), together with additional functional complementation data in other model organisms (*39*, *40*), suggest that Vangl1 and Vangl2 have identical tissue-specific biochemical activities.

So far, two *Lp* alleles have been described, the naturally occurring *Lp* and the chemically induced *Lp*^{m1Jus} (*5*, *6*). Sequence analysis revealed the presence of independent *Vangl2* mutations in both alleles, namely, D255E (*Lp*^{m1Jus}) and S464N (*Lp*), both of which map to the predicted cytoplasmic domain of the protein (*5*−*7*). The similar phenotypes in vivo of embryos heterozygotes and homozygotes for each mutant suggest that both mutations behave as loss-of-function in a gene dosage dependent pathway. The mechanistic and molecular basis for the loss-of-function in these proteins in vivo and in vitro remains largely unknown and was investigated in the present study. For this, we stably expressed the wild type protein and the D255E *Lp*-associated mutant variant in Madin-Darby canine kidney (MDCK) cells and studied the effect of D255E on protein expression, stability, maturation, subcellular localization, and cell surface expression.

MATERIAL AND METHODS

Material and Antibodies. Cycloheximide was purchased from Sigma-Aldrich (St-Louis, MO). MG132 was from Calbiochem (San Diego, CA). Geneticin (G418), penicillin, and streptomycin were obtained from Invitrogen (Carlsbad, CA). All the restriction enzymes were from New England Biolabs (Ipswich, MA). Taq DNA polymerase was from Invitrogen (Carlsbad, CA). The mouse monoclonal antibodies directed against the influenza hemagglutin epitope (HA.11) and the c-Myc epitope were purchased from Covance (Berkeley, CA). The mouse monoclonal antibody recognizing Na,K-ATPase (alpha) was from Santa Cruz Biotechnology (Santa Cruz, CA). The mouse monoclonal anti-BiP antibody was from BD Biosciences (San Jose, CA). The rabbit polyclonal antibodies against calnexin and PDI (Protein Disulfide Isomerase) were from Stressgen (Ann Arbor, MI). The rabbit polyclonal antibody against calreticulin was obtained from Affinity BioReagents (Golden, CO). Cy3-conjugated goat anti-mouse and anti-rabbit antibodies and peroxidase-coupled goat anti-mouse antibody were from Jackson ImmunoResearch Laboratories (West Grove, PA).

Plasmids and Constructs. The human *Vangl1* cDNA was amplified from total human RNA by RT-PCR and cloned into the pCS2+ vector. The D255E mutation was introduced in the human *Vangl1* cDNA by PCR overlap extension mutagenesis, followed by subcloning into pCS2+. PCR was used to insert a short antigenic epitope (EQKLISEEDL) from the human c-Myc protein at the N-terminus of Vangl1 wild type (WT) and Vangl1 D255E sequences, using oligonucleotides 5′-CAAGAAGAATTCATG**GAGCAGAAGCTAATCTCTGAGGAGGATCTG**GATACCGAATCCACTTATTC-3′ (forward *Vangl1* primer with the c-Myc epitope sequence in bold) and 5′-CTCTTGTCTAGATTAAACGGATGTCTCAGACTG-3′ (reverse *Vangl1* primer). The recombinant c-Myc tagged cDNAs were reconstructed using unique *Eco*RI and *XbaI* sites (underlined) present in the primers, followed by cloning into the corresponding sites of the pCB6 expression vector. For the cell surface quantification of Vangl1 protein expression, an hemagglutinin (HA) epitope (YPYDVPDYA) was inserted immediately after amino acid position 139 of Vangl1 WT and Vangl1 D255E, using PCR mutagenesis with primers: 5′-**TACCCATACGATGTGCCAGACTACGCT**AGCGATGAGCTGGAGCCTTGTGGCACAATTTGT-3′ (forward Vangl1-HA139) and 5′-GCT**AGCGTAGTCTGGCACATCGTATGGGTA**CCTCCACAGGATCGGAGGTAAAAGGATGAA-3′ (reverse Vangl1-HA139), with HA coding sequences in bold. To enable insertion of additional adjacent HA epitope(s), a NheI restriction site was inserted at the 3′-end of the HA sequence, accounting for the additional Ser residue found at the end of the HA tag. To facilitate identification of transfected cells expressing recombinant Vangl1 proteins, c-Myc tagged *Vangl1* cDNAs were fused in-frame to the green fluorescent protein (GFP) by cloning the various *Vangl1 EcoRI-XbaI* PCR fragments into peGFP-C1 vector (Clontech, Mountain View, CA) modified to accommodate the in-frame insertion of the *Eco*RI-*XbaI Vangl1* wild type, *Vangl1* HA139, *Vangl1* D255E, and *Vangl1* HA139+D255E PCR fragments.

Cell Culture and Transfection. Madin-Darby canine kidney (MDCK) epithelial cells were maintained in Dulbecco's modified Eagle's medium (DMEM) supplemented with 10% fetal bovine serum (FBS), 100 units/mL penicillin, and 100 μg/mL streptomycin at 37 °C in a 5% CO_2 incubator. For stable transfection, MDCK cells were transfected with Vangl1 constructs subcloned in peGFP-C1 using Lipofectamine Plus Reagent (InVitrogen). Selection for stably transfected clones was done in growth medium containing 0.4 mg/mL G418 for 10−14 days. Expression of recombinant GFP-Vangl1 variants was initially identified by fluorescence microscopy on live cells and confirmed by Western blotting analysis. Total cell lysates were prepared in RIPA buffer (50 mM Tris-HCl pH 7.5, 150 mM NaCl, 5 mM EDTA, 1% Triton X-100 supplemented with protease inhibitors), cleared by passage through a 25G needle and centrifugation at 13 000 rpm for 10 min (4 °C). Cell lysates (50 μg) were separated by electrophoresis using 7.5% SDS−polyacrylamide gels, followed by electroblotting and incubation with the monoclonal anti-c-Myc antibody 9E10 (used at 1:500). Immune complexes were revealed with a horseradish peroxidase conjugated goat anti-mouse antibody (1:10000) and visualized by enhanced chemiluminescence (SuperSignal West Pico kit, Thermo Scientific Rockford, IL).

Crude Membrane Preparation. Crude membrane fractions from stably transfected MDCK cells expressing GFP-Vangl1 WT and D255E were prepared as described (*41*). Cells seeded in three 150-mm dishes were grown to confluence; they were then washed once in ice-cold phosphate buffered saline (PBS) and once in cold NTE buffer (10 mM Tris-HCl pH 7.5, 100 mM NaCl, 10 mM EDTA) and promptly harvested by scrapping in

Tris-Mg buffer (10 mM Tris-HCl pH 7.5, 1 mM $MgCl_2$ with protease inhibitors) followed by homogenization using a Dounce homogenizer (50 strokes on ice). Unbroken cells and nuclei were removed by centrifugation (500g for 5 min), and a crude membrane fraction was prepared by centrifugation of the supernatant fraction at 50000g for 30 min. The pellet containing the membrane proteins was resuspended in NTE buffer supplemented with protease inhibitors. The supernatant containing the cytosolic proteins was also harvested for analysis.

Quantification of Cell Surface Expression by Enzyme-Linked Immunosorbent Assay. Quantification of cell surface expression of HA-tagged GFP-Vangl1 proteins was done by enzyme-linked immunosorbent assay as described previously (*42*). Briefly, MDCK cells stably transfected with HA-tagged Vangl1 WT or D255E were grown to confluence in 24-well plates and fixed with 4% paraformaldehyde for 20 min. Cells were blocked in 5% nonfat milk in PBS for 30 min, incubated with mouse anti-HA Ab (1:200 dilution) for 1 h, washed and incubated with HRP conjugated goat anti-mouse Ab (1:4000 dilution) for 1 h. For quantification of total HA-tagged GFP-Vangl1, cells were permeabilized with 0.1% Triton X-100 in PBS for 30 min prior to incubation with anti-HA Ab. Peroxidase activity was quantified colorimetrically using the HRP substrate [0.4 mg/mL *O*-phenylenediamine dihydrochloride (OPD), Sigma-Aldrich] according to the manufacturer's instructions. Absorbance readings (492 nm) were taken in an ELISA plate reader and background absorbance reading from nonspecific binding of primary antibody to vector-transfected cells were subtracted for each sample. Cell surface reading were normalized to total HA-tagged GFP-Vangl1 value for each cell clone and were expressed as a percentage.

Metabolic Labeling, Pulse-Chase Study, and Immunoprecipitation. Confluent MDCK cells stably expressing GFP-Vangl1 WT and D255E proteins seeded on 60 mm dishes were preincubated 90 min at 37 °C in methionine- and cysteine-free DMEM media containing 10% dialyzed FBS (labeling media). Thereafter, cells were pulsed-labeled for 60 min at 37 °C with 2 mL of labeling media containing 100 μCi of [^{35}S] methionine-cysteine (Perkin-Elmer, Boston, MA). Cells were then washed twice with PBS and incubated in 2 mL of chase medium (standard DMEM containing 10% FBS, 15 μg/mL methionine, and 15 μg/mL cysteine) for up to 8 h. Cells were lysed in 400 μL of RIPA buffer. For immunoprecipitation, equal amounts of cell lysates were adjusted to 1 mg/mL in RIPA buffer and incubated with the mouse anti-Myc antibody 9E10 (2.5 μg) overnight at 4 °C, followed by incubation with protein A/G-sepharose (GE Healthcare, Piscataway, NJ) for 4 h. Beads were washed three times in RIPA buffer and proteins were eluted with 50 μL of 2× sample buffer. The radiolabeled proteins were separated by electrophoresis using 7.5% SDS polyacrylamide gels. The gels were then fixed, impregnated with Amplify (GE Healthcare, Piscataway, NJ), dried, and exposed to film. Densitometric analysis was performed by using NIH ImageJ software (NIH, Bethesda, MD).

Determination of Relative Protein Stability using Cycloheximide Chase. To determine the stability of both GFP-Vangl1 WT and D255E proteins, MDCK cells expressing these proteins were treated with cycloheximide (20 μg/mL). At predetermined time points, cells were harvested, lysed with RIPA buffer, and subjected to SDS−PAGE and immunoblot analysis. Signal intensities were quantitated using NIH ImageJ software, with actin or tubulin used as internal controls.

Immunofluorescence and Confocal Microscopy. To examine subcellular localization (permeabilized conditions), MDCK cells stably expressing different Vangl1 constructs were seeded at high density onto glass coverslips in a 24-well plate. Twenty-four hours later, cells were washed twice with ice-cold PBS, fixed for 15−20 min in 4% paraformaldehyde (PFA) in PBS, and then permeabilized with 0.5% Triton X-100 in PBS for 15 min. After blocking nonspecific binding with 5% goat serum and 0.1% bovine serum albumin (BSA) in PBS for 1 h, the cells were incubated with the desired primary antibody [mouse anti-Na,K-ATPase (1:100); mouse anti-HA (1:200); rabbit anti-calreticulin (1:100)] for 1 h and washed three times with 0.1% BSA in PBS. Finally, the coverslips were incubated for 1 h with the appropriate secondary antibody [goat anti-mouse-Cy3 (1:1000); goat anti-rabbit-Cy3 (1:1000)] and washed three times with 0.1% BSA in PBS. All the incubations were done at room temperature and the antibodies were all diluted in blocking solution. To detect cell surface expression of the exofacial HA epitope engineered in Vangl1 proteins (nonpermeabilized conditions), MDCK cells expressing HA-tagged GFP-Vangl1 WT and D255E were incubated with the mouse anti-HA (1:200) in DMEM containing 2% nonfat milk for 2 h at 37 °C. After several washes with PBS, cells were fixed for 15 min with 4% PFA in PBS and incubated with goat anti-mouse-Cy3 antibody (1:1000) for 1 h. For immunofluorescence, coverslips were rinsed once in water and mounted by using Permafluor Aqueous Mounting Medium (Thermo Scientific, Fremont, CA). Confocal microscopy was done using a Zeiss LSM5 Pascal laser scanning confocal microscope. All image analyses were performed using the LSM5 Image software. To maximize image quality, a Median filter 3 × 3 was applied to the images using Image-Pro software. To remove out-of-focus fluorescence, the Z stack sections were also deconvoluted using 10 iterations with the AutoQuant software.

RESULTS

Expression and Subcellular Localization of Vangl1 WT and D255E in MDCK Cells. Targeting of the Vangl1 protein to the cell membrane is thought to be critical for biological function in vivo, including the formation of membrane associated multisubunit PCP signaling complexes (*25*, *43*, *44*). To investigate the possible effect of the *Lp*-associated pathogenic mutation D255E on this and other aspects of Vangl1 protein structure and function, we stably expressed wild type (WT) and D255E Vangl1 protein in MDCK cells. This cell type was chosen, since it is derived from a lineage that normally expresses Vangl proteins in vivo during kidney tubulogenesis (*8*) and is therefore likely to possess the cellular machinery required for proper expression, maturation, membrane insertion, and subcellular targeting of the protein.

To facilitate detection in transfected cells, the WT *Vangl1* cDNAs were first modified by in-frame addition of GFP at the amino terminus and also with the insertion of the antigenic c-Myc for fluorescence localization and immunoblotting, respectively (Figure 1A). Several stably transfected MDCK clones were identified by GFP fluorescence, and Vangl1 protein expression was confirmed by immunoblotting analysis (data not shown).

Total cell extracts and crude membrane fractions were prepared from two independent MDCK Vangl1 WT transfectants and were analyzed by immunoblotting (anti-c-Myc antibody; Figure 1B). A specific immunoreactive species of ~80 kDa was

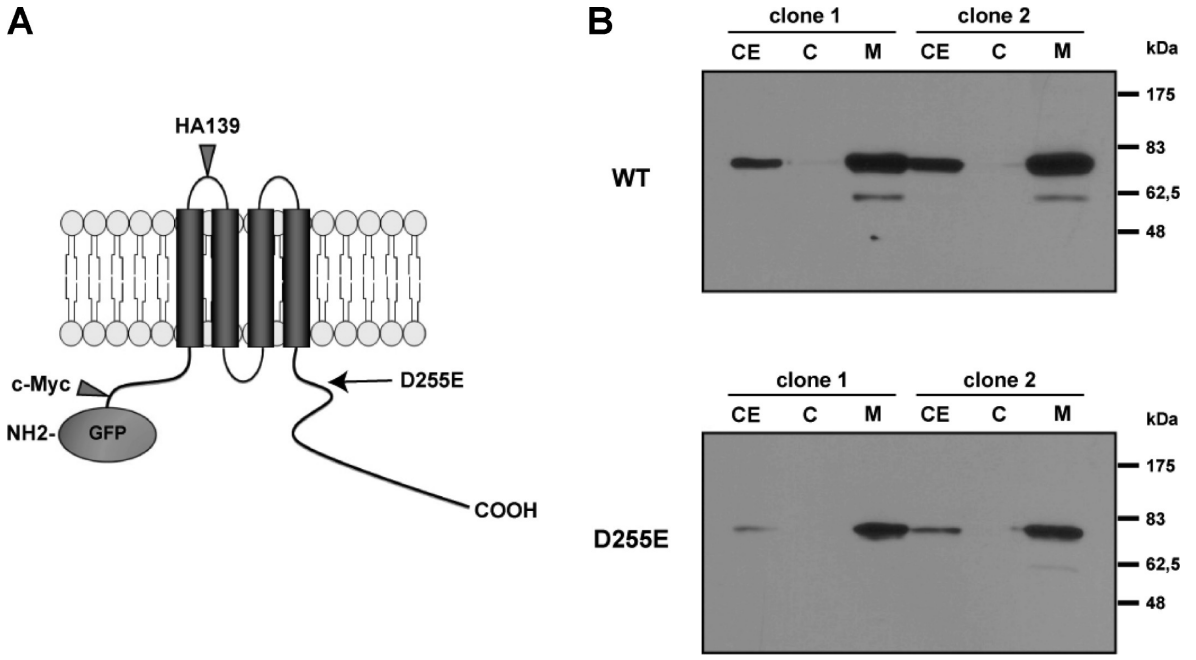

FIGURE 1: Expression of WT and D255E Vangl1 variant in the membrane fraction of transfected MDCK cells. (A) Schematic representation of the GFP-Vangl1 protein including positions of the hemagglutin (HA) tag inserted at position 139 (predicted TM1-TM2 connecting loop), the c-Myc tag inserted in the amino-terminal segment, GFP at the N-terminus and the D255E mutation in the intracellular C-terminal region. (B) Independent MDCK cell clones stably expressing either WT or D255E mutant variant (reconstructed in human GFP-Vangl1 protein) were isolated. Total cell extracts (CE), membrane-enriched fractions (M), and soluble cytoplasmic extracts (C) were prepared from these cells and equal amounts of protein (50 μg) were analyzed by immunoblotting with the mouse monoclonal antibody 9E10 directed against the c-Myc tag inserted in-frame near the amino terminus of the recombinant proteins.

detected in total cell extracts, in agreement with the predicted molecular mass of the GFP-tagged protein (Figure 1B; top panel). This species was greatly enriched in crude membrane extracts but was absent from cytoplasmic fractions. These results suggest that the GFP-Vangl1 WT protein is associated with membrane in the stable MDCK cell clones.

The Vangl1 D255E mutant fused to GFP was also stably expressed in MDCK cells and the effect of the mutation on various structural and functional properties of Vangl1 was investigated. Several D255E expressing MDCK cell clones were initially identified by GFP fluorescence, and total cell extracts, crude membrane, and cytosolic fractions were analyzed by immunoblotting (Figure 1B; bottom panel). As for WT Vangl1, D255E was found to be highly enriched in the membrane fraction of these transfectants, suggesting that D255E does not impair membrane association of the Vangl1 protein. On the other hand, we systematically observed in multiple transfected clones a lower overall level expression of the D255E variant compared to WT (Figure 1B, Supplemental Figure S2, Supporting Information and data not shown).

The subcellular localization of GFP-Vangl1 WT was analyzed by confocal microscopy. As opposed to the cytoplasmic fluorescence signal detected in MDCK cells expressing control GFP (Figure 2; top panels), GFP-Vangl1 MDCK transfectants showed strong localization of the GFP fluorescence at the membrane (Figure 2; middle panels), producing a typical mesh-like signal in confluent cell monolayers. In addition, the GFP-Vangl1 signal was found to fully colocalize with Na,K-ATPase, a specific marker for basolateral membrane of MDCK cells (Figure 2; middle panels). Taken together, results in Figures 1B and 2 show that GFP-tagged Vangl1 is mainly expressed at the plasma membrane of MDCK cell clones.

To detect a possible effect of the D255E mutation on the subcellular distribution and plasma membrane (PM) targeting of Vangl1, the cellular localization of Vangl1 D255E in MDCK cells was also analyzed by confocal microscopy and compared to that of the WT protein (Figure 2; bottom panels). By contrast to WT Vangl1 that shows a clear PM-associated signal, D255E signal did not appear concentrated at the PM, but rather showed an intracellular punctate pattern suggestive of localization to an intracellular endomembrane compartment. In addition, D255E did not colocalize with the PM marker Na,K-ATPase. The seemingly distinct subcellular localization of the WT and D255E proteins was confirmed by examination of cell sections (Z stacks) (Figure 3). These studies showed that the WT Vangl1 is expressed predominantly at the basal and lateral membranes of polarized MDCK cells (Figure 3A − top panel and Supplemental Figure S1, Supporting Information), where it shows complete colocalization with the basolateral membrane marker Na, K-ATPase (Figure 3A − middle and bottom panels). However, a similar analysis of D255E expressing cells showed that the mutant variant is not detected at the basolateral membrane and does not colocalize with Na,K-ATPase; the D255E signal is largely limited to an intracellular compartment (Figure 3B and Supplemental Figure S1, Supporting Information). Together, these results strongly suggest that the pathogenic D255E mutation interferes with normal subcellular targeting of the protein.

Surface Expression of Vangl1 Proteins in MDCK Cells. Results in Figure 3 show that in polarized MDCK cells, WT Vangl1 is expressed at the basolateral membrane. It is anticipated that in younger, nonpolarized cultures of MDCK cells, WT Vangl1 will be broadly present at the cell surface. To detect possible surface expression of WT Vangl1 in nonpolarized MDCK cells, we engineered an exofacial HA antigenic epitope at position 139 located in the first predicted extracellular loop of Vangl1 (delineated by the predicted TM1-TM2 segments). The mutant D255E was similarly modified by HA tag addition and

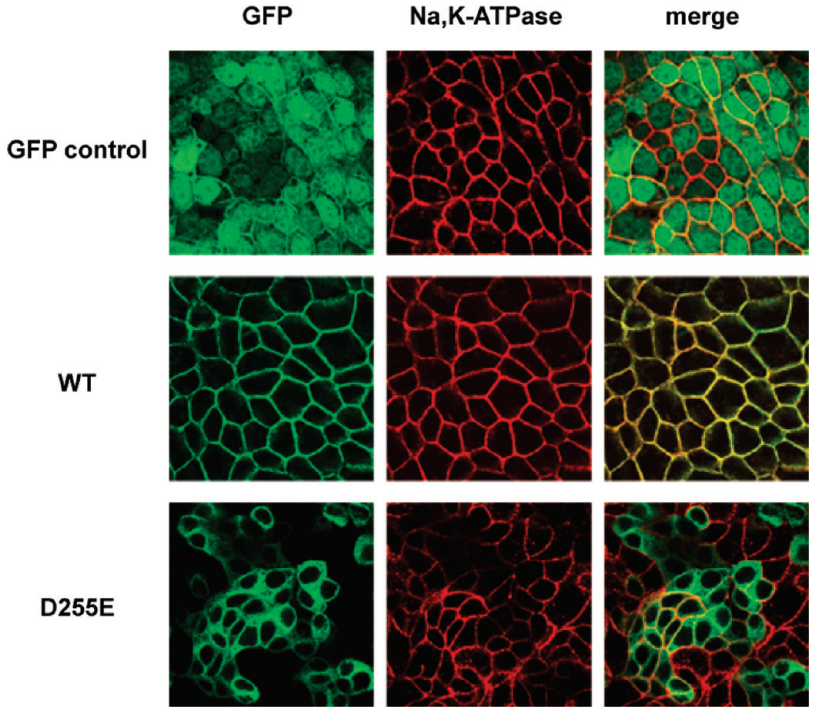

FIGURE 2: Cellular localization of WT and D255E Vangl1 proteins in transfected MDCK cells. Transfected MDCK cells stably expressing GFP alone, GFP-Vangl1 WT, and GFP-Vangl1 D255E (green) were grown to confluence, fixed, permeabilized, and stained for Na,K-ATPase followed by Cy3-conjugated secondary antibody (red), and examined by confocal microscopy. The merge images show that while the majority of GFP-Vangl1 WT signal is associated to the plasma membrane and overlaps with Na,K-ATPase (yellow), the GFP-Vangl1 D255E staining is mostly intracellular with little if any colocalization with Na,K-ATPase. Images are representative of at least three independent experiments of each type.

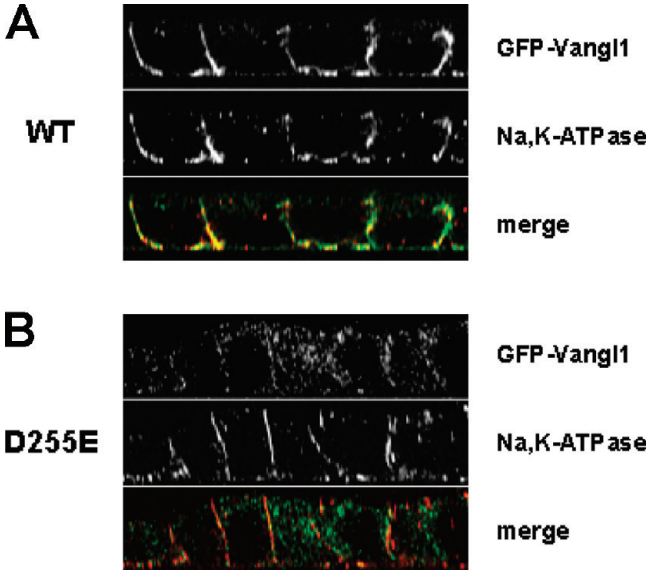

FIGURE 3: Cellular localization of the D255E mutant Vangl1 variant in stably transfected MDCK cells; Z-line image analysis. Transfected MDCK cells stably expressing either GFP-Vangl1 WT (A) or the D255E mutant variant (B) were processed as described in the legend to Figure 2. Cells were analyzed by confocal microscopy to visualize the expression of GFP-Vangl1 (green) and Na,K-ATPase (red). Representative X−Z sections are shown. The merge images show that while GFP-Vangl1 WT colocalizes with Na,K-ATPase at the basolateral membrane (yellow) of the polarized cells, the D255E mutant does not and is mainly localized to an intracellular compartment.

analyzed in parallel. The polarity of the HA tag with respect to PM was determined by immunofluorescence with an anti-HA antibody used in intact cells (extracellular) and in cells permeabilized with Triton X-100 (intracellular) (Figure 4), as we have previously described (*41*, *42*). A strong fluorescence signal was detected in both permeabilized and nonpermeabilized MDCK clones expressing WT Vangl1 (Figure 4A); this signal was absent from control untransfected MDCK cells similarly exposed to the anti-HA antibody (data not shown). These results indicate that the inserted HA tag is surface accessible and strongly suggest that a) WT Vangl1 is expressed at the cell surface of nonpolarized MDCK cells and b) that the protein segment delineated by predicted TM1-TM2 is indeed extracytoplasmic. By contrast, MDCK clones expressing the D255E variant displayed bright intracellular fluorescence in permeabilized cells (Figure 4A bottom − left), but showed no fluorescence under nonpermeabilized conditions (Figure 4A bottom − right), suggesting that D255E is not expressed at the cell surface of MDCK cells. The presence/absence of immunoreactive HA tag at the cell surface of MDCK cells expressing WT or D255E proteins was also investigated by an ELISA based assay (*42*). For this, corresponding MDCK transfectants were fixed and incubated with anti-HA antibody with or without prior permeabilization. The amount of bound anti-HA antibody was quantified using a secondary antibody coupled to horseradish peroxidase. Cells expressing WT Vangl1-HA analyzed in this manner were found to express 93 ± 6% of total immunoreactive Vangl1 at the cell surface (Figure 4B), while only a small fraction of D255E was detected at the cell surface (14% ± 1%). Together, results in Figures 2−4 show that the D255E mutation disrupts normal subcellular localization of Vangl1 and interferes with normal PM targeting of the protein.

Stability of the D255E Variant in MDCK Cells. The overall lower level of the D255E variant detected in transfected MDCK cells (compared to WT; Figure 1B, Supplemental Figure S2, Supporting Information and data not shown), together with the noted defect in subcellular targeting of the variant prompted us to analyze a possible effect of the mutation on protein half-life

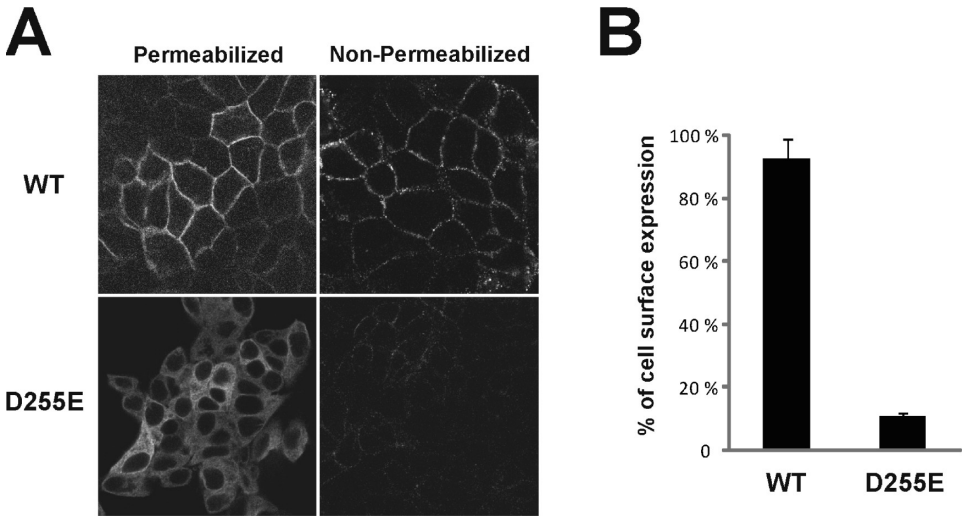

FIGURE 4: Analysis of plasma membrane targeting and surface expression of WT and D255E Vangl1 variants in MDCK cells. (A) MDCK cells stably expressing either HA-tagged GFP-Vangl1 WT or D255E were analyzed by immunofluorescence to detect surface expression of an HA antigenic epitope inserted at position 139 in the predicted TM1-TM2 connecting loop. Immunofluorescence was carried out on either intact cells (nonpermeabilized, right panel) or in cells pretreated with 0.1% Triton-X-100 (permeabilized; left panel), using a mouse anti-HA antibody. Cells were incubated with Cy3-conjugated secondary antibody and images were acquired by confocal microscopy. Images are representative of at least three independent experiments of each type. (B) In other experiments, the same cells exposed to the anti-HA antibody were incubated with an HRP-coupled secondary anti-mouse antibody and the amount of the primary antibody present was determined for both conditions (permeabilized and nonpermeabilized) by a colorimetric reaction using an HRP substrate quantitated by spectrometry. The amount of HA-tagged GFP-Vangl1 WT and D255E proteins expressed at the cell surface (detected in nonpermeabilized cells) is shown as a fraction (%) of total protein expression (measured in permeabilized cells).

and stability. For this, MDCK transfectants expressing WT or D255E variants were treated with cycloheximide to block protein synthesis, and the fate of the mature protein was monitored over time by immunoblotting analysis of corresponding cell lysates harvested at predetermined time-points (Figure 5). Using this approach, we determined that the half-life of WT Vangl1 expressed in MDCK cells was ~9 h, while that of the D255E variant was ~2 h. Eight hours of incubation with cycloheximide resulted in almost complete disappearance (~ 95%) of D255E, while > 50% of the WT protein was still detectable in cells similarly treated. The stability of WT and D255E Vangl1 proteins was also investigated by pulse-chase experiments. MDCK clones were labeled with ^{35}S-methione/cysteine for 60 min (pulse) and the fate of the radiolabeled proteins was followed for 8 h by immunoprecipitation using extracts from pulsed cells grown in isotope-free medium (chase). Representative autoradiograms and quantification from three independent experiments are shown in Figure 6A and B, respectively. In these experiments, the half-life of WT Vangl1 in MDCK cells was estimated to be > 13 h, while the half-life of D255E was found to be significantly shorter than ~4 h. Results from these experiments agree with that monitoring protein stability following exposure to cycloheximide and strongly suggest that the D255E mutation causes a strong decrease in protein stability.

ER Retention of Vangl1 D255E Protein. The reduced half-life, the absence of PM targeting, and the localization of the D255E variant to a subcellular endomembrane compartment suggested that the D255E may have a defect in maturation associated with retention of the protein in the endoplasmic reticulum (ER). This possibility was tested by immunofluorescence using an antibody directed against the ER marker calreticulin. MDCK cells expressing WT Vangl1 showed an absence of overlap between the PM-associated GFP fluorescence (GFP-Vangl1) and the intracellular punctate ER staining produced by calreticulin (Figure 7 − top panels). In contrast, there was significant colocalization of D255E and calreticulin, suggesting that D255E is indeed present predominantly in the ER endomembrane compartment (Figure 7 − middle and bottom panels). Retention of inappropriately folded proteins in the ER, including membrane proteins, ultimately leads to their degradation by the proteasome (*45*). To analyze proteasome-mediated proteolytic degradation of Vangl1, MDCK cells expressing WT or D255E were exposed to cycloheximide (CHX) (up to 8 h) either in the presence or absence of the proteasome inhibitor MG132 (Figure 8 and Supplemental Figure S2, Supporting Information). Cell extracts were prepared and analyzed by immunoblotting, and the amount of immunoreactive Vangl1 protein was quantified. As previously shown in Figure 5, CHX treatment of WT and D255E expressing cells had a differential effect on the level of Vangl1 protein remaining after 8 h of treatment, with a > 90% decrease in D255E variant, compared to only a small reduction in the amount of WT protein. On the other hand, MG132-mediated proteasome inhibition of CHX-treated cells resulted in a dramatic increase in the amount of detectable D255E variant (~60% of untreated controls) in these cell extracts. MG132/CHX treatment also resulted in a modest increase of detectable WT protein (when compared to CHX treatment alone). Furthermore, the addition of chloroquine, a lysosome inhibitor, did not prevent the rapid degradation of D255E (Supplemental Figure S2, Supporting Information). Together, these results suggest that D255E is retained in the ER, where it is targeted for degradation in a proteasome-dependent manner.

The presence of misfolded proteins in the ER may induce the unfolded protein response (UPR), which involves the upregulation of the expression of genes encoding ER-resident chaperones, for example, BiP (*46*). If D255E was recognized by the cell as a misfolded protein, it should trigger the UPR when expressed in cells. To analyze UPR activation, we measured the expression of ER chaperones (BiP, calnexin, and PDI) by Western blotting in MDCK cells expressing WT and D255E. No differences were

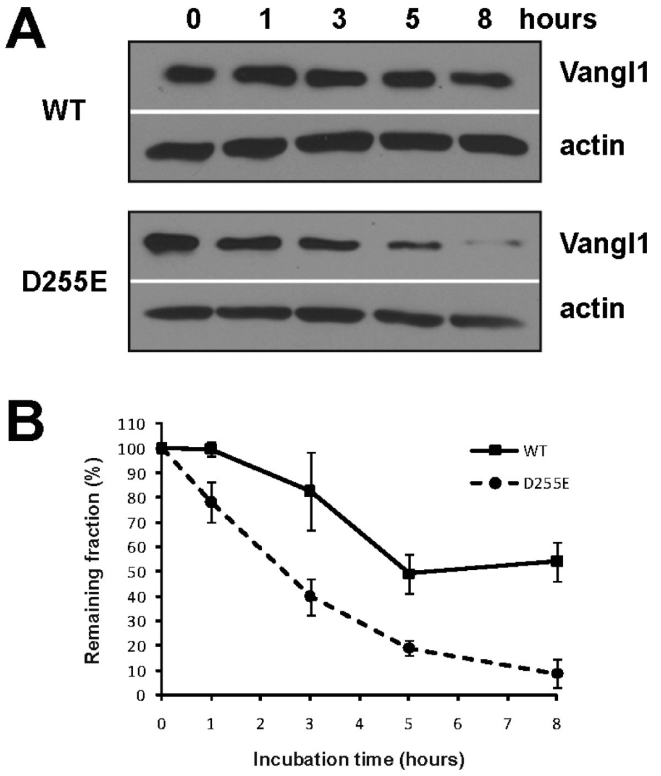

FIGURE 5: Stability of GFP-Vangl1 WT and D255E proteins in MDCK cells. (A) MDCK cells stably expressing either GFP-Vangl1 WT or D255E were grown to confluence and treated with cycloheximide (20 μg/mL) for the indicated time. Cell lysates (50 μg) were analyzed by immunoblotting using the anti-c-Myc antibody 9E10. Actin was used as an internal loading control and was detected using a rabbit polyclonal antiserum. To obtain comparable signal intensity at T0, the GFP-Vangl1 D255E blots were exposed for longer times. (B) Estimation of the rate of disappearance of GFP-Vangl1 WT and D255E. The Vangl1 signal from multiple immunoblots (mean ± SE of 4−9 experiments) was quantified (pixel density of each band) and is expressed as a fraction (%) of the untreated sample which is set at 100%.

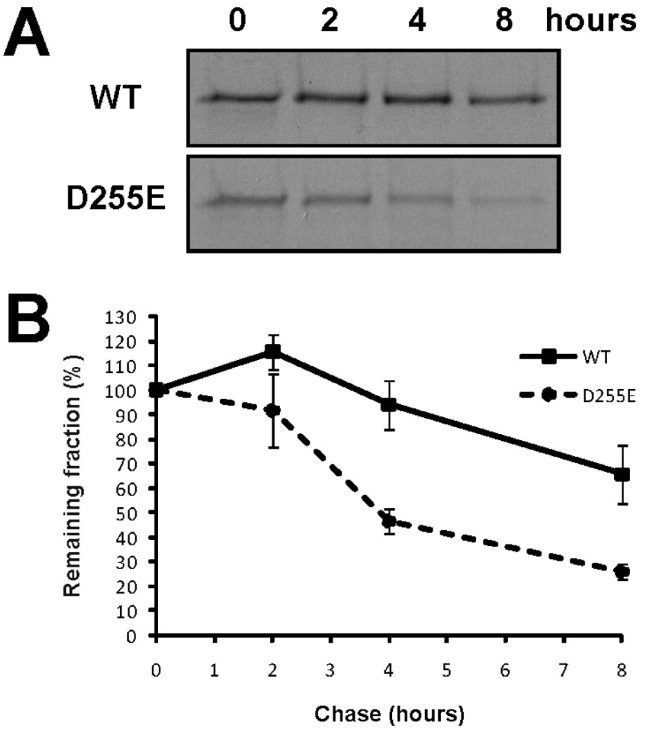

FIGURE 6: Pulse-chase studies of GFP-Vangl1 WT and D255E proteins expressed in MDCK cells. (A) MDCK cells stably expressing either GFP-Vangl1 WT or D255E were metabolically labeled by a 60-min pulse of ^{35}S-Met/Cys. The cells were transferred to radioactivity-free complete medium, followed by different chase periods. Cell lysates were prepared and subjected to Vangl1 immunoprecipitation followed by gel electrophoresis and autoradiography. To obtain comparable signal intensity at T0, the GFP-Vangl1 D255E blots were exposed for longer times. (B) Estimation of the rate of disappearance of GFP-Vangl1 WT and D255E labeled proteins. The amount of radiolabeled Vangl1 WT and D255E proteins was deduced from scanning the autoradiograms as described in the legend to Figure 5. The graph represents the mean of three experiments ± SE.

seen in the expression of BiP, calnexin, and PDI between the different cell lines (Supplemental Figure S2, Supporting Information), indicating that UPR is not activated in MDCK cells expressing D255E Vangl protein.

DISCUSSION

Vangl1 and Vangl2 are mammalian homologues of the *Drosophila* Van Gogh (Vang) or Strabismus (Stbm) proteins (*12*, *13*). The two proteins share ~70% sequence similarity, including a 4 TM domains predicted structure with intracellular amino and carboxy termini. In *Drosophila*, *Vang*/*Stbm* belongs to the PCP gene family (*14*, *15*, *47*, *48*), and is involved in the coordination of polarization of cells within the epithelial plane. In vertebrates, a clear example of PCP is the alignment and orientation of stereocilia in neurosensory cells of the cochlea (organ of Corti) (*28*, *33*−*35*, *49*, *50*) and mutations in *Vangl1* (*37*) and *Vangl2* (*8*, *34*) disrupt polarity of these stereociliary bundles (*51*). Moreover, studies in *Xenopus* and subsequently in other vertebrates showed that alterations in the Vangl genes cause defects in CE movements during embryogenesis (*34*, *49*, *52*, *53*). In mammals, CE movements play a critical role in a number of developmental pathways such as neural tube closure, kidney tubulogenesis, as well as biogenesis of the cardiovascular system (*8*, *54*−*56*). Indeed, mice carrying mutations in *Vangl1* (*37*) and *Vangl2* (*5*−*7*) show severe craniorachischisis, as well as other malformations, most notably in the heart and large blood vessels (*37*, *56*, *57*). Finally, studies in normal mouse embryos by our lab (*8*) and others (*28*, *58*) have shown that Vangl proteins are expressed at the cell membrane in a number of epithelial cell lineages throughout embryonic development. Together, these results indicate that proper biogenesis of Vangl proteins, including targeting to the membrane, plays a critical role in the establishment of PCP and in CE movements in mammals.

The biochemical characteristics of Vangl proteins remain largely unknown. Likewise, their molecular mechanism of action both during normal embryogenesis and in the case of pathogenic mutations (*Lp*) associated with NTDs, are poorly understood. For these studies, human VANGL1 was used as a molecular backbone; this was to anchor potential future characterization of the rare VANGL1 variants recently identified in human cases of spina bifida (*38*, *39*), in the biochemical framework described here. Although the pathogenic D255E mutation studied here emerged in Vangl2, much data indicate that Vangl1 and Vangl2 proteins are functionally equivalent and that the choice of the molecular backbone should not impact the biochemical characterization of pathogenic mutations. Indeed, the two proteins are structurally highly similar, and expression of the zebrafish *Vangl1* (*40*) or human *VANGL1* (*59*) in zebrafish *tri*/*Vangl2* mutants can correct the CE defect of these mutant animals. In addition, loss-of-function mutations in mouse *Vangl1* and *Vangl2*

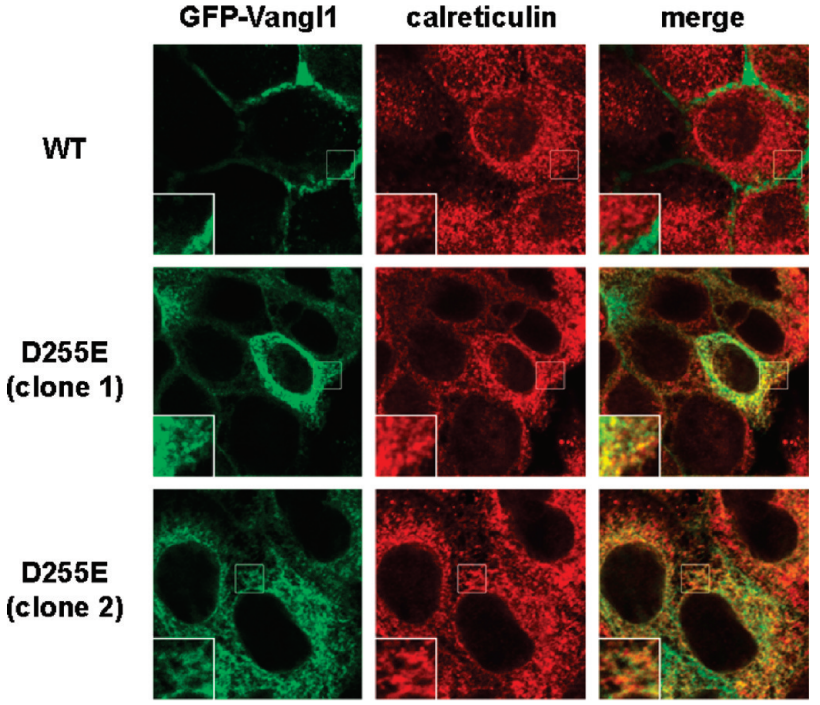

FIGURE 7: Determination of subcellular localization of Vangl1 D255E by double immunofluorescence. MDCK cells stably expressing either GFP-Vangl1 WT or the D255E (clone 1 and clone 2) were fixed and immunostained for the endoplasmic reticulum marker calreticulin (red). As opposed to GFP-Vangl1 WT which is expressed at the plasma membrane, the mutant GFP-Vangl1 D255E shows intracellular staining that significantly overlaps with calreticulin. Insets are magnifications of the indicated areas.

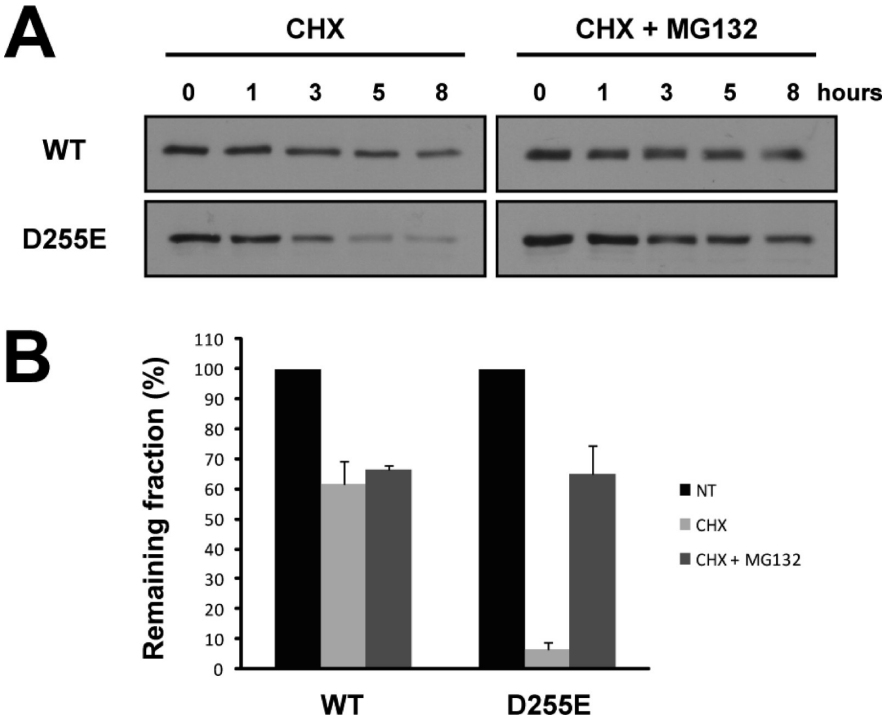

FIGURE 8: Proteasome-mediated degradation of WT and D255E Vangl1 expressed in MDCK cells. (A) MDCK cells stably expressing either GFP-Vangl1 WT or D255E were grown to confluence and treated with cycloheximide (20 μg/mL) for various time periods, either in the absence or presence of the proteasome inhibitor MG132 (5 μg/mL). Cell lysates (50 μg) were subjected to gel electrophoresis and immunoblotting for Vangl1 using the anti-c-Myc antibody. Tubulin was used as an internal loading control (not shown). To obtain comparable signal intensity at T0, the GFP-Vangl1 D255E blots were exposed for longer times. (B) The effect of MG132 on the stability of the WT and D255E mutant after 8 h of treatment was quantitated by densitometry scanning as described in the legend of Figure 5. Each value represents mean ± SE of 5−6 independent experiments.

show the same PCP defect in vivo (*37*). Finally, the *Lp*-associated D255E mutation abrogates Vangl interaction with Dvl1, Dvl2, and Dvl3, when reconstructed in either Vangl1 or Vangl2 (*9*). The biochemical characterization of Vangl1 reported here thus provides an experimental framework to study the molecular basis of loss-of-function mutations in the Vangl proteins.

We have stably expressed WT Vangl1 protein (fused to GFP) in MDCK cells and observed that Vangl1 is mainly expressed at the plasma membrane. Furthermore, using an exofacial HA antigenic epitope inserted between the predicted TM1 and TM2, we show that this portion of the protein is exposed to the extracellular milieu, where it is available for possible interactions with other proteins. The extracytoplasmic localization of the TM1-TM2 segment demonstrated here also supports the topological model predicted by hydropathy profiling that we proposed previously (*9*). In polarized cultures of MDCK cells, Vangl1 is expressed at the basolateral membrane, where it colocalizes with Na,K-ATPase. This restricted basolateral expression is similar to the subcellular localization that we observed for Vangl1 and Vangl2 in the inner ear of mouse embryos (*37*). Moreover, we also demonstrated that Vangl2 was detected mostly at the cell membrane in several tubular structures of mouse embryos, including developing kidney, esophagus, and skin (*8*). This comparable pattern of expression indicates that MDCK cells represent an appropriate host to study the biochemical properties of Vangl proteins, including maturation, processing, and membrane targeting.

Comparative analysis of the NTD-associated D255E revealed that the mutation has multiple and complex effects on the biochemical properties of the protein. First, the expression of the D255E variant is greatly reduced at the plasma membrane or at the basolateral membrane of polarized MDCK, but is majorly found in an endomembrane compartment that shows overlapping staining with the ER marker calreticulin. This suggests a major defect in maturation and targeting of the D255E variant. Concomitant with altered subcellular localization, we observed that the D255E mutation causes a dramatic reduction in protein stability, both at steady state (reduced expression in transfectants) and in pulse-chase studies where a 2 h half-life was noted compared to >9 h for the WT protein. Finally, reduced stability of the D255E variant is also accompanied by rapid, MG132-sensitive, proteasome-dependent degradation of the mutant. Together, these results suggest that the D255E mutation causes misfolding of the protein which is associated with a failure to mature and in the accumulation of the mutant variant in the ER. The D255E variant appears unstable and is rapidly targeted for degradation by the proteasome. The overall net effect is that D255E is predominantly not expressed at the plasma membrane, thereby strongly suggesting that it cannot participate in the formation of PCP signaling complexes. While the current manuscript was under review, another study published by Merte et al. supports our claim that the D255E mutation interferes with the targeting of the protein at the cell surface. They showed that the Vangl2 D255E protein fails to become recruited by COPII vesicles and leads to its retention in the ER (*60*). The properties of the D255E mutant including instability, ER retention, and failure to reach the site of biological function (plasma membrane) are likely to result in a complete loss-of-function variant. Such behavior and associated null phenotype has been previously described for pathogenic mutations in a number of other membrane proteins, for example, Pgp (ABCB1) (*61*), CFTR (ABCC7) (*62*), and Slc11a2 (Nramp2) (*63*). Although we favor a model in which D255E causes a general defect in protein folding, it is also possible that D255E affects a targeting signal required for protein sorting and trafficking to the plasma membrane. Sequence analysis reveals the presence of putative basolateral targeting motifs in the N-terminus ($YSGF_{10}$, $YSYY_{13}$) and downstream TM4 ($YKDF_{287}$) of Vangl1. Furthermore, a dileucine motif, known to be required for endocytosis, but sometimes also for basolateral sorting, is found in the N-terminus of Vangl1 (LL_{57}). However, D255E does not affect any of these signatures.

In the absence of high resolution three-dimentional structure of Vangl proteins, one can only speculate on the effect of the D255E on Vangl protein stucture, including the associated folding/maturation defect of this variant. D255 maps to the large C-terminal intracellular domain of the protein, aproximately 10 residues downstream TM4 and is absolutely conserved (invariant) in all Vangl proteins sequenced to date, from flies to humans. Although D255 is not part of any recognizable signature or structural motif, its high degree of conservation suggests an important role. Moreover, the nature of the substitution at D255 that causes loss-of-function in vivo is highly conservative, replacing an aspartate by a glutamate; this substitution preserves the negatively charged carboxylate, while introducing a modest change in the size of the carbon side chain. The fact that a highly conservative change at that position has such a profound effect on protein structure and function also suggest a critical role for this residue and domain in protein folding and stability, including possible interaction with other proteins required for maturation.

The complex biochemical defect of the D255E variant characterized herein explains a number of in vivo observations on the behavior of the mutant. Using immunofluorescence on sections of neural tubes from E10.5 embryos, we have detected reduced overall expression level and decreased apparent plasma membrane expression of D255E in neurepithelial cells of *Lp*/*Lp* embryos compared to WT (*8*). Likewise, in hair cells of the cochlea, membrane staining of both Vangl2 and associated Dvl2 is disrupted in *Lp*/*Lp* (D255E) embryos (*49*), the latter possibly through impaired binding to Vangl2. These findings are consistent with the severe targeting defect of D255E detected here in MDCK cells. In addition, we have shown that the C-terminal portion (251−526) of Vangl1 and Vangl2 physically interacts with the N-terminal portion (containing the DIX and PDZ domains) of the three Dvl proteins (Dvl1, 2, and 3) and that the D255E mutation abrogates this interaction (*9*). The major effect of the D255E mutation on protein stability detected in MDCK cells (including possible misfolding and retention in the ER) would also explain the loss of interaction with Dvl proteins detected by yeast two hybrid analysis (*9*).

Lp/+ heterozygous mouse exhibits a mild looped tail phenotype, whereas *Lp*/*Lp* homozygotes exhibit both a looped tail and craniorachischisis (*4*−*6*). This codominant phenotype is the same for both known alleles at *Lp*, namely, *Lp* (S464N) and Lp^{m1Jus} (D255E)(*5*). The codominance nature of the *Lp* defect can be explained either by (a) a partial or complete loss of function of the mutant gene/protein in a gene dosage dependent pathway or (b) a gain of function associated with a dominant negative effect. Our results strongly suggest that D255E is a loss-of-function mutation. We believe that Vangl proteins form part of a gene dosage dependent pathway critical for neural tube formation. This is also supported by the observations that mice doubly heterozygote for loss of function at *Vangl1* and *Vangl2* ($Vangl1^{+/-}$:$Vangl2^{Lp/+}$) show the same severe craniorachischisis NTD as $Vangl2^{Lp/Lp}$ homozygotes (*37*). However, one cannot formally exclude the possibility that D255E represents a gain-of-function mutation, with the mutant variant exerting a dominant negative effect on the WT protein. In such a scenario, D255E would interfere with normal maturation or targeting of the WT protein produced in

the same cells. This hypothesis is supported by the report that Vangl proteins can form multimers (*64*). Additional studies will be required to clarify this point.

Taken together, our finding of improper targeting of the D255E mutation associated with NTDs in mice suggests that this conserved residue in both Vangl1 and Vangl2 plays an important role in correct protein folding/targeting. Consequently, the absence of the Vangl proteins at the plasma membrane disrupts the PCP pathway and causes major developmental defects, such as neural tube defect. Identifying protein determinants responsible for targeting of Vangl proteins to the plasma membrane and elucidating the mechanistic basis of loss of function in mutant variants associated with NTD in mice and human may help in understanding the mechanism by which Vangl1 and Vangl2 proteins control cell polarity and CE movements.

ACKNOWLEDGMENT

We thank Drs. Elena Torban, Alan Underhill, Doug Epstein, and Sergio Grinstein for their thoughtful comments on the manuscript. Image acquisition, data analysis, and image processing were done on equipment and with the assistance of the McGill Life Sciences Complex Imaging Facility which is funded by the Canadian Foundation for Innovation.

SUPPORTING INFORMATION AVAILABLE

Confocal analysis of GFP-Vangl1 WT and D255E localization in MDCK cells; Western blot analysis of the degradation of WT and D255E proteins, and determination of the expression levels of UPR markers in MDCK cells expressing WT and D255E. This material is available free of charge via the Internet at http://pubs.acs.org.

REFERENCES

1. Frey, L., and Hauser, W. A. (2003) Epidemiology of neural tube defects. *Epilepsia 44* (Suppl 3), 4–13.
2. Copp, A. J., Greene, N. D., and Murdoch, J. N. (2003) Dishevelled: linking convergent extension with neural tube closure. *Trends Neurosci. 26*, 453–455.
3. Copp, A. J., Greene, N. D., and Murdoch, J. N. (2003) The genetic basis of mammalian neurulation. *Nat. Rev. Genet. 4*, 784–793.
4. Strong, L. C., and Hollander, W. F. (1949) Hereditary loop-tail in the house mouse. *J. Heredity 40*, 329–334.
5. Kibar, Z., Underhill, D. A., Canonne-Hergaux, F., Gauthier, S., Justice, M. J., and Gros, P. (2001) Identification of a new chemically induced allele (Lp(m1Jus)) at the loop-tail locus: morphology, histology, and genetic mapping. *Genomics 72*, 331–337.
6. Kibar, Z., Vogan, K. J., Groulx, N., Justice, M. J., Underhill, D. A., and Gros, P. (2001) Ltap, a mammalian homolog of Drosophila Strabismus/Van Gogh, is altered in the mouse neural tube mutant Loop-tail. *Nat. Genet. 28*, 251–255.
7. Murdoch, J. N., Doudney, K., Paternotte, C., Copp, A. J., and Stanier, P. (2001) Severe neural tube defects in the loop-tail mouse result from mutation of Lpp1, a novel gene involved in floor plate specification. *Hum. Mol. Genet. 10*, 2593–2601.
8. Torban, E., Wang, H. J., Patenaude, A. M., Riccomagno, M., Daniels, E., Epstein, D., and Gros, P. (2007) Tissue, cellular and sub-cellular localization of the Vangl2 protein during embryonic development: effect of the Lp mutation. *Gene Expr. Patterns 7*, 346–354.
9. Torban, E., Wang, H. J., Groulx, N., and Gros, P. (2004) Independent mutations in mouse Vangl2 that cause neural tube defects in looptail mice impair interaction with members of the Dishevelled family. *J. Biol. Chem. 279*, 52703–52713.
10. Darken, R. S., Scola, A. M., Rakeman, A. S., Das, G., Mlodzik, M., and Wilson, P. A. (2002) The planar polarity gene strabismus regulates convergent extension movements in Xenopus. *EMBO J. 21*, 976–985.
11. Jessen, J. R., Topczewski, J., Bingham, S., Sepich, D. S., Marlow, F., Chandrasekhar, A., and Solnica-Krezel, L. (2002) Zebrafish trilobite identifies new roles for Strabismus in gastrulation and neuronal movements. *Nat. Cell Biol. 4*, 610–615.
12. Taylor, J., Abramova, N., Charlton, J., and Adler, P. N. (1998) Van Gogh: a new Drosophila tissue polarity gene. *Genetics 150*, 199–210.
13. Wolff, T., and Rubin, G. M. (1998) Strabismus, a novel gene that regulates tissue polarity and cell fate decisions in Drosophila. *Development 125*, 1149–1159.
14. Fanto, M., and McNeill, H. (2004) Planar polarity from flies to vertebrates. *J. Cell Sci. 117*, 527–533.
15. Klein, T. J., and Mlodzik, M. (2005) Planar cell polarization: an emerging model points in the right direction. *Annu. Rev. Cell Dev. Biol. 21*, 155–176.
16. Chae, J., Kim, M. J., Goo, J. H., Collier, S., Gubb, D., Charlton, J., Adler, P. N., and Park, W. J. (1999) The Drosophila tissue polarity gene starry night encodes a member of the protocadherin family. *Development 126*, 5421–5429.
17. Feiguin, F., Hannus, M., Mlodzik, M., and Eaton, S. (2001) The ankyrin repeat protein Diego mediates Frizzled-dependent planar polarization. *Dev Cell 1*, 93–101.
18. Gubb, D., Green, C., Huen, D., Coulson, D., Johnson, G., Tree, D., Collier, S., and Roote, J. (1999) The balance between isoforms of the prickle LIM domain protein is critical for planar polarity in Drosophila imaginal discs. *Genes Dev. 13*, 2315–2327.
19. Jenny, A., Reynolds-Kenneally, J., Das, G., Burnett, M., and Mlodzik, M. (2005) Diego and Prickle regulate Frizzled planar cell polarity signalling by competing for Dishevelled binding. *Nat. Cell Biol. 7*, 691–697.
20. Klingensmith, J., Nusse, R., and Perrimon, N. (1994) The Drosophila segment polarity gene dishevelled encodes a novel protein required for response to the wingless signal. *Genes Dev. 8*, 118–130.
21. Theisen, H., Purcell, J., Bennett, M., Kansagara, D., Syed, A., and Marsh, J. L. (1994) dishevelled is required during wingless signaling to establish both cell polarity and cell identity. *Development 120*, 347–360.
22. Usui, T., Shima, Y., Shimada, Y., Hirano, S., Burgess, R. W., Schwarz, T. L., Takeichi, M., and Uemura, T. (1999) Flamingo, a seven-pass transmembrane cadherin, regulates planar cell polarity under the control of Frizzled. *Cell 98*, 585–595.
23. Strutt, D. I. (2002) The asymmetric subcellular localisation of components of the planar polarity pathway. *Semin. Cell Dev. Biol. 13*, 225–231.
24. Axelrod, J. D. (2001) Unipolar membrane association of Dishevelled mediates Frizzled planar cell polarity signaling. *Genes Dev. 15*, 1182–1187.
25. Bastock, R., Strutt, H., and Strutt, D. (2003) Strabismus is asymmetrically localised and binds to Prickle and Dishevelled during Drosophila planar polarity patterning. *Development 130*, 3007–3014.
26. Das, G., Jenny, A., Klein, T. J., Eaton, S., and Mlodzik, M. (2004) Diego interacts with Prickle and Strabismus/Van Gogh to localize planar cell polarity complexes. *Development 131*, 4467–4476.
27. Tree, D. R., Shulman, J. M., Rousset, R., Scott, M. P., Gubb, D., and Axelrod, J. D. (2002) Prickle mediates feedback amplification to generate asymmetric planar cell polarity signaling. *Cell 109*, 371–381.
28. Montcouquiol, M., Sans, N., Huss, D., Kach, J., Dickman, J. D., Forge, A., Rachel, R. A., Copeland, N. G., Jenkins, N. A., Bogani, D., Murdoch, J., Warchol, M. E., Wenthold, R. J., and Kelley, M. W. (2006) Asymmetric localization of Vangl2 and Fz3 indicate novel mechanisms for planar cell polarity in mammals. *J. Neurosci. 26*, 5265–5275.
29. Wallingford, J. B., Fraser, S. E., and Harland, R. M. (2002) Convergent extension: the molecular control of polarized cell movement during embryonic development. *Dev Cell 2*, 695–706.
30. Carreira-Barbosa, F., Concha, M. L., Takeuchi, M., Ueno, N., Wilson, S. W., and Tada, M. (2003) Prickle 1 regulates cell movements during gastrulation and neuronal migration in zebrafish. *Development 130*, 4037–4046.
31. Goto, T., and Keller, R. (2002) The planar cell polarity gene strabismus regulates convergence and extension and neural fold closure in Xenopus. *Dev. Biol. 247*, 165–181.
32. Wallingford, J. B., and Harland, R. M. (2002) Neural tube closure requires Dishevelled-dependent convergent extension of the midline. *Development 129*, 5815–5825.
33. Curtin, J. A., Quint, E., Tsipouri, V., Arkell, R. M., Cattanach, B., Copp, A. J., Henderson, D. J., Spurr, N., Stanier, P., Fisher, E. M., Nolan, P. M., Steel, K. P., Brown, S. D., Gray, I. C., and Murdoch, J. N. (2003) Mutation of Celsr1 disrupts planar polarity of inner ear

hair cells and causes severe neural tube defects in the mouse. *Curr. Biol. 13*, 1129–1133.
34. Montcouquiol, M., Rachel, R. A., Lanford, P. J., Copeland, N. G., Jenkins, N. A., and Kelley, M. W. (2003) Identification of Vangl2 and Scrb1 as planar polarity genes in mammals. *Nature 423*, 173–177.
35. Wang, Y., Guo, N., and Nathans, J. (2006) The role of Frizzled3 and Frizzled6 in neural tube closure and in the planar polarity of inner-ear sensory hair cells. *J. Neurosci. 26*, 2147–2156.
36. Katoh, Y., and Katoh, M. (2005) Comparative genomics on Vangl1 and Vangl2 genes. *Int. J. Oncol. 26*, 1435–1440.
37. Torban, E., Patenaude, A. M., Leclerc, S., Rakowiecki, S., Gauthier, S., Andelfinger, G., Epstein, D. J., and Gros, P. (2008) Genetic interaction between members of the Vangl family causes neural tube defects in mice. *Proc. Natl. Acad. Sci. U. S. A. 105*, 3449–3454.
38. Kibar, Z., Bosoi, C. M., Kooistra, M., Salem, S., Finnell, R. H., De Marco, P., Merello, E., Bassuk, A. G., Capra, V., and Gros, P. (2009) Novel mutations in VANGL1 in neural tube defects. *Hum. Mutat. 30*, E706–715.
39. Kibar, Z., Torban, E., McDearmid, J. R., Reynolds, A., Berghout, J., Mathieu, M., Kirillova, I., De Marco, P., Merello, E., Hayes, J. M., Wallingford, J. B., Drapeau, P., Capra, V., and Gros, P. (2007) Mutations in VANGL1 associated with neural-tube defects. *N. Engl. J. Med. 356*, 1432–1437.
40. Jessen, J. R., and Solnica-Krezel, L. (2004) Identification and developmental expression pattern of van gogh-like 1, a second zebrafish strabismus homologue. *Gene Expr. Patterns 4*, 339–344.
41. Kast, C., and Gros, P. (1998) Epitope insertion favors a six transmembrane domain model for the carboxy-terminal portion of the multidrug resistance-associated protein. *Biochemistry 37*, 2305–2313.
42. Czachorowski, M., Lam-Yuk-Tseung, S., Cellier, M., and Gros, P. (2009) Transmembrane topology of the mammalian Slc11a2 iron transporter. *Biochemistry 48*, 8422–8434.
43. Jenny, A., and Mlodzik, M. (2006) Planar cell polarity signaling: a common mechanism for cellular polarization. *Mt. Sinai J. Med. 73*, 738–750.
44. Park, M., and Moon, R. T. (2002) The planar cell-polarity gene stbm regulates cell behaviour and cell fate in vertebrate embryos. *Nat. Cell Biol. 4*, 20–25.
45. Ellgaard, L., and Helenius, A. (2003) Quality control in the endoplasmic reticulum. *Nat. Rev. Mol. Cell Biol. 4*, 181–191.
46. Austin, R. C. (2009) The unfolded protein response in health and disease. *Antioxid. Redox Signaling 11*, 2279–2287.
47. Wang, Y., and Nathans, J. (2007) Tissue/planar cell polarity in vertebrates: new insights and new questions. *Development 134*, 647–658.
48. Zallen, J. A. (2007) Planar polarity and tissue morphogenesis. *Cell 129*, 1051–1063.
49. Wang, J., Mark, S., Zhang, X., Qian, D., Yoo, S. J., Radde-Gallwitz, K., Zhang, Y., Lin, X., Collazo, A., Wynshaw-Boris, A., and Chen, P. (2005) Regulation of polarized extension and planar cell polarity in the cochlea by the vertebrate PCP pathway. *Nat. Genet. 37*, 980–985.
50. Chacon-Heszele, M. F., and Chen, P. (2009) Mouse models for dissecting vertebrate planar cell polarity signaling in the inner ear. *Brain Res. 1277*, 130–140.
51. Jones, C., and Chen, P. (2007) Planar cell polarity signaling in vertebrates. *Bioessays 29*, 120–132.
52. Murdoch, J. N., Henderson, D. J., Doudney, K., Gaston-Massuet, C., Phillips, H. M., Paternotte, C., Arkell, R., Stanier, P., and Copp, A. J. (2003) Disruption of scribble (Scrb1) causes severe neural tube defects in the circletail mouse. *Hum. Mol. Genet. 12*, 87–98.
53. Park, T. J., Gray, R. S., Sato, A., Habas, R., and Wallingford, J. B. (2005) Subcellular localization and signaling properties of dishevelled in developing vertebrate embryos. *Curr. Biol. 15*, 1039–1044.
54. Ybot-Gonzalez, P., Savery, D., Gerrelli, D., Signore, M., Mitchell, C. E., Faux, C. H., Greene, N. D., and Copp, A. J. (2007) Convergent extension, planar-cell-polarity signalling and initiation of mouse neural tube closure. *Development 134*, 789–799.
55. McNeill, H. (2009) Planar cell polarity and the kidney. *J. Am. Soc. Nephrol. 20*, 2104–2111.
56. Etheridge, S. L., Ray, S., Li, S., Hamblet, N. S., Lijam, N., Tsang, M., Greer, J., Kardos, N., Wang, J., Sussman, D. J., Chen, P., and Wynshaw-Boris, A. (2008) Murine dishevelled 3 functions in redundant pathways with dishevelled 1 and 2 in normal cardiac outflow tract, cochlea, and neural tube development. *PLoS Genet. 4*, e1000259.
57. Phillips, H. M., Rhee, H. J., Murdoch, J. N., Hildreth, V., Peat, J. D., Anderson, R. H., Copp, A. J., Chaudhry, B., and Henderson, D. J. (2007) Disruption of planar cell polarity signaling results in congenital heart defects and cardiomyopathy attributable to early cardiomyocyte disorganization. *Circ. Res. 101*, 137–145.
58. Saburi, S., Hester, I., Fischer, E., Pontoglio, M., Eremina, V., Gessler, M., Quaggin, S. E., Harrison, R., Mount, R., and McNeill, H. (2008) Loss of Fat4 disrupts PCP signaling and oriented cell division and leads to cystic kidney disease. *Nat. Genet. 40*, 1010–1015.
59. Reynolds, A., McDearmid, J. R., Lachance, S., Marco, P. D., Merello, E., Capra, V., Gros, P., Drapeau, P., Kibar, Z. VANGL1 rare variants associated with neural tube defects affect convergent extension in zebrafish, Mech. Dev. In Press, doi:10.1016/j.mod.2009.12.002.
60. Merte, J., Jensen, D., Wright, K., Sarsfield, S., Wang, Y., Schekman, R., and Ginty, D. D. (2010) Sec24b selectively sorts Vangl2 to regulate planar cell polarity during neural tube closure. *Nat. Cell Biol. 12*, 41–46.
61. Ambudkar, S. V., Kim, I. W., and Sauna, Z. E. (2006) The power of the pump: mechanisms of action of P-glycoprotein (ABCB1). *Eur. J. Pharm. Sci. 27*, 392–400.
62. Cheung, J. C., and Deber, C. M. (2008) Misfolding of the cystic fibrosis transmembrane conductance regulator and disease. *Biochemistry 47*, 1465–1473.
63. Lam-Yuk-Tseung, S., Camaschella, C., Iolascon, A., and Gros, P. (2006) A novel R416C mutation in human DMT1 (SLC11A2) displays pleiotropic effects on function and causes microcytic anemia and hepatic iron overload. *Blood Cells Mol. Dis. 36*, 347–354.
64. Bellaiche, Y., Beaudoin-Massiani, O., Stuttem, I., and Schweisguth, F. (2004) The planar cell polarity protein Strabismus promotes Pins anterior localization during asymmetric division of sensory organ precursor cells in Drosophila. *Development 131*, 469–478.